The Strong MRI Relaxivity of Paramagnetic Nanoparticles

ARTICLE *in* THE JOURNAL OF PHYSICAL CHEMISTRY B · JUNE 2008

Impact Factor: 3.3 · DOI: 10.1021/jp8012706 · Source: PubMed

THE JOURNAL OF PHYSICAL CHEMISTRY B LETTERS

2008, *112,* 6288–6291
Published on Web 04/24/2008

The Strong MRI Relaxivity of Paramagnetic Nanoparticles

Gengmei Xing, Hui Yuan, Rui He, Xueyun Gao,* Long Jing, Feng Zhao, Zhifang Chai, and Yuliang Zhao*,§

Lab for Bio-Environmental Effects of Nanomaterials and Nanosafety, Institute of High Energy Physics, Chinese Academy of Science, Beijing, 100049, and National Center for Nanosciences and Technology, 100080, Beijing, China

Received: February 2, 2008; Revised Manuscript Received: March 24, 2008

We developed a method to synthesize paramagnetic nanoparticles of $Gd@C_{82}(OH)_{22\pm2}$. Such nanoparticles are with ordered microstructures and have strong MRI proton relaxation in vitro/vivo. Compared with commercial Gd-DTPA, a 12× MRI relaxivity of $Gd@C_{82}(OH)_{22\pm2}$ nanoparticles with ordered microstructures was achieved in vitro. The small $Gd@C_{82}(OH)_{22\pm2}$ nanoparticles, ~65nm, could easily escape the RES uptake in vivo; this opens the door for their clinical applications.

Magnetic resonance imaging (MRI) desires new contrast agents with high proton relaxivity. Recently, great efforts have been made to explore nanostructure-based MRI contrast agents like $Gd@C_{2n}$ derivatives.[1–6] Wilson et al. showed an important result that the $Gd@C_{60}(OH)_x$ could aggregate into a water-soluble paramagnetic particle that has size-dependent MRI relaxivity in vitro;[4] in simplicity, the larger $Gd@C_{60}(OH)_x$ particles have higher relaxivity. For example, $Gd@C_{60}(OH)_x$ particles with a diameter of ~810nm had the longitudinal relaxation rate (r_1) of ~83.2 mM^{-1} sec^{-1}, but when the particle size decreased to ~90.9 nm, the r_1 dramatically decreased to 14.1 mM^{-1} s^{-1}.[5] A similar result was reported for $Gd@C_{82}(OH)_x$ when it was utilized as the MRI contrast agent by Shinohara et al.[5,6] However, no studies were carried on the relation between relaxivity and microstructures of the metallofullerene nanoparticles. As the microstructures of such nanoparticles may be an important factor to influence their longitudinal relaxation rate (r_1) in MRI,[4] researchers should explore how microstructures of paramagnetic particles influence their relaxivity. This may help us to find some small paramagnetic nanoparticles (with sizes below 100 nm) with stronger proton relaxivity due to their specific microstructures. In clinical applications, the paramagnetic particles with sizes below ~100 nm and higher r_1 values are really desired[7–10] because such small particles can escape the uptake of the reticuloendothelial system (RES) in the liver, lung, and spleen in vivo, which results in a strong MRI signal in the diagnosis target organ/tissue.[11,12]

To prepare metallofullerene nanoparticles with a well-controlled microstructure, we have developed a method to synthesize high-quality $Gd@C_{82}(OH)_x$ (99.5% purity) and found that a narrower range of hydroxyl numbers on the surface of $Gd@C_{82}(OH)_x$ is very important for controlling the microstructure and size of $Gd@C_{82}(OH)_x$ nanoparticles in aqueous solution. Further, a medium number of hydroxyl groups ($x \sim 20$) on $Gd@C_{82}(OH)_x$ is another key factor for achieving the biocompatibility, solubility, and stability of $Gd@C_{82}(OH)_x$.[13,14] We first isolated the $Gd@C_{82}(OH)_{22\pm2}$ from the $Gd@C_{82}(OH)_x$ mixture. To optimize the quality of $Gd@C_{82}(OH)_{22\pm2}$ nanoparticles, we further controlled the size and microstructure of $Gd@C_{82}(OH)_{22\pm2}$ in solution via pH modulation. The methods to synthesize and characterize $Gd@C_{82}(OH)_{22\pm2}$ and control the formation of nanoparticles in aqueous solution are described in the Supporting Information (S1, S2, S3, S4).

The size and morphology of the prepared $Gd@C_{82}(OH)_{22\pm2}$ particles are observed by AFM and shown in Figure 1a (pH 2), b(pH 5), and c (pH 7); see details in The Supporting Information (S5). Figure 1a shows that $Gd@C_{82}(OH)_{22\pm2}$ (pH 2) nanoparticles are well-dispersed on a mica substrate with average sizes of 95 ± 15 nm. The morphology of the particle is quasi-sphere but not very uniform. Figure 1b reveals that the nanoparticles (pH 5) are well-deposited on mica with a diameter of 76 ± 12 nm, and Figure 1c discloses that the particles (pH 7) were well-spread with diameters of 65 ± 10 nm. We further investigated the microstructures of these particles by a high-resolution transmission electron microscope (HRTEM; see details in the Supporting Information S6). The HRTEM images of the $Gd@C_{82}(OH)_{22\pm2}$ nanoparticle at pH 2 show a typical structure of disordered patterns (Figure 1d). At pH 5, the ratio of the ordered pattern increased when compare with that for the pH 2 particle, but there is still no uniform pattern (Figure 1e). However, $Gd@C_{82}(OH)_{22\pm2}$ self-assembled into a hexagonal pattern at pH 7 (Figure 1f). Further HRTEM analysis confirmed that most $Gd@C_{82}(OH)_{22\pm2}$ nanoparticles at pH 7 formed a similar microstructure. In general, the AFM studies showed that the size of $Gd@C_{82}(OH)_{22\pm2}$ at different pHs is in the order 95 (pH 2) > 76 (pH 5) > 65 nm (pH 7). HRTEM also disclosed that the quality of nanoparticles at pH 7 is better than that of samples at pH 2 or pH 5. The $Gd@C_{82}(OH)_{22\pm2}$ nanoparticles dispersed in solution were further studied by the small-angle X-ray scattering (SAXS) method in the Beijing Synchrotron Radiation Laboratory, and the SAXS results reveal that the $Gd@C_{82}(OH)_{22\pm2}$ nanoparticles in solution are similar in size

* To whom correspondence should be addressed. Tel: 86-10-88233191. E-mail: zhaoyuliang@ihep.ac.cn (Y.Z.); Tel: 86-10-88236709. E-mail: gaoxy@ihep.ac.cn (W. G.).
§ National Center for Nanosciences and Technology.

10.1021/jp8012706 CCC: $40.75

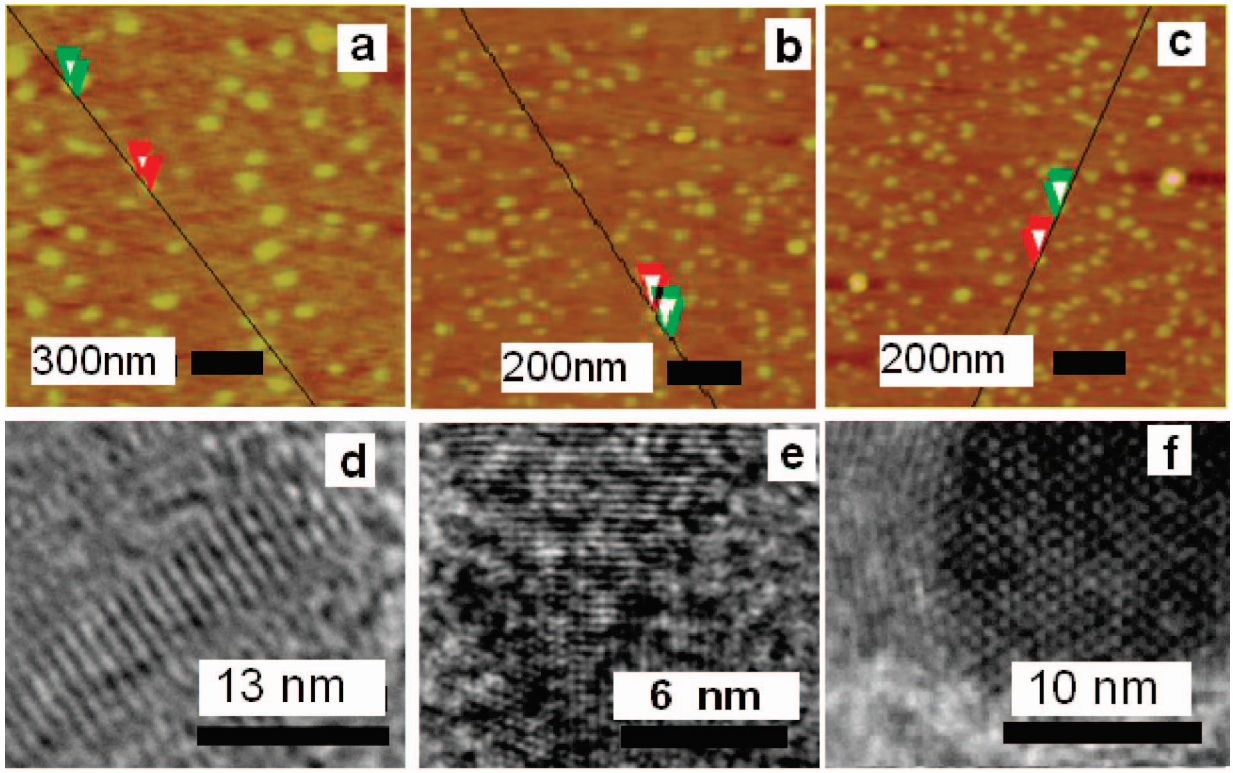

Figure 1. AFM images of Gd@$C_{82}(OH)_{22\pm2}$ nanoparticles at (a) pH 2, (b) pH 5, and (c) pH 7. HRTEM images of Gd@$C_{82}(OH)_{22\pm2}$ nanoparticles at (d) pH 2, (e) pH 5, and (f) pH 7.

when compared with the aforementioned AFM and TEM observations (see details in the Supporting Information S7).

Why do the Gd@$C_{82}(OH)_{22\pm2}$ molecules aggregate together to form a paramagnetic nanoparticle as shown in Figure 1? We give a plausible speculation that follows. It is known that Gd is off-centered in the cage and that its three electrons are transferred to the carbon cage, in which the carbons close to Gd have rich electron density and are easily hydroxylated. This will induce the added hydroxyls to be localized on the carbon cage close to Gd.[15] As a result, the Gd@$C_{82}(OH)_{22\pm2}$ likes amphiphilic molecules where one side has hydrophilic OH groups and the other side is the hydrophobic carbon cage. The amphiphilic Gd@$C_{82}(OH)_{22\pm2}$ would easily self-assemble in aqueous solution and form particles. Note that hydroxyl groups of Gd@$C_{82}(OH)_{22\pm2}$ nanoparticles will be protonated or deprotonated at different pHs. This will vary the negative charges of hydroxyl groups, which further modulates the repulsive static-electric force among Gd@$C_{82}(OH)_{22\pm2}$ species. Obviously, this repulsive static-electric force will affect the hydrophobic-force-induced self-assembly of Gd@$C_{82}(OH)_{22\pm2}$. To reveal this assumption, zeta potentials of 0.05 mM Gd@$C_{82}(OH)_{22\pm2}$ solutions at different pHs were checked with a Zetasizer 3000HS (see Supporting Information S8 for details). At pH 7, Gd@$C_{82}(OH)_{22\pm2}$ is negatively charged, with a zeta potential of −11 mV due to some protons of the OH groups moving into solution. At pH 5, the zeta potentials of Gd@$C_{82}(OH)_{22\pm2}$ are −5 mV because some protons attach to the O^- in the hydroxyl groups as the solution becomes acidic. The zeta potential of Gd@$C_{82}(OH)_{22\pm2}$ at pH 2 is −2 mV as more protons absorb on the hydroxyl groups when the solution pH becomes lower. At pH 7, the repulsive static-electric force and hydrophobic interactions among Gd@$C_{82}(OH)_{22\pm2}$ species would modulate their self-assembly well in a benign way and result in small Gd@$C_{82}(OH)_{22\pm2}$ nanoparticles with ordered microstructures; see Figure 1f. However, in acidic solution (pH 5 and

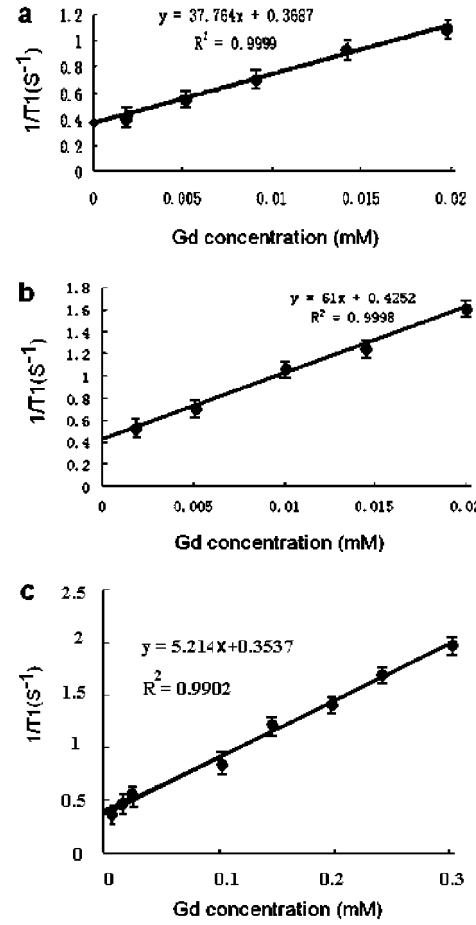

Figure 2. The longitudinal relaxation rate (r_1) of Gd@$C_{82}(OH)_{22\pm2}$ nanoparticles at (a) pH 2 and (b) pH 7 and (c) r_1 of Gd-DTPA. At 25 °C, the relaxivities of all samples were determined at a resonance frequency of 200 MHz on a 4.7 T/30 cm Biospec MRI scanner from Bruker.

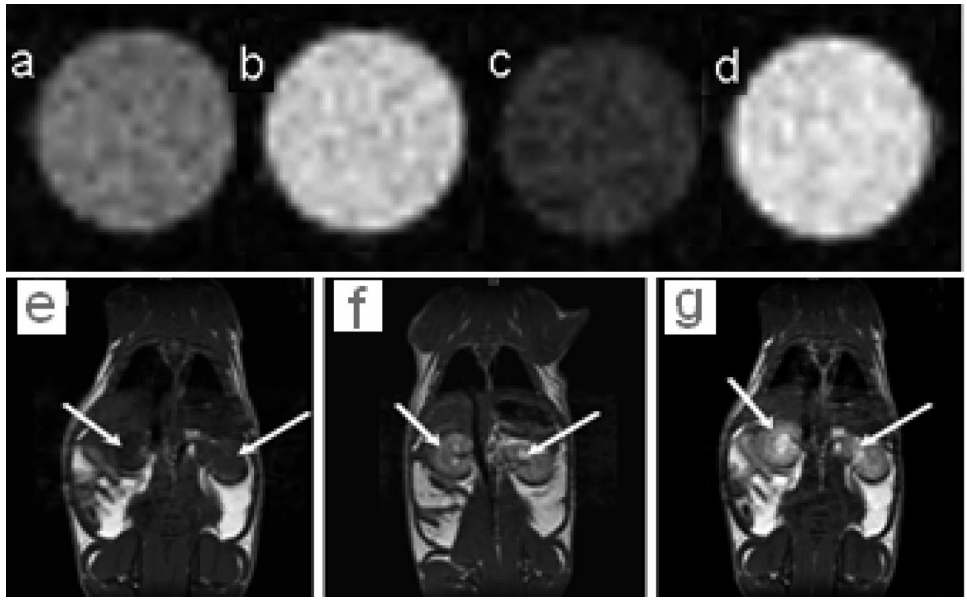

Figure 3. T1-weighted MRI of $Gd@C_{82}(OH)_{22\pm2}$ nanoparticles and Gd-DTPA in vitro and vivo. (a) $Gd@C_{82}(OH)_{22\pm2}$ nanoparticles at ~0.05 mM at pH 2 in vitro. (b) $Gd@C_{82}(OH)_{22\pm2}$ nanoparticles at ~0.05 mM at pH 7 in vitro. (c) Gd-DTPA at ~0.05 mM in vitro. (d) Gd-DTPA at ~1 mM in vitro. (e) MRI of mice before i.v. administration of $Gd@C_{82}(OH)_{22\pm2}$ nanoparticles. (f) MRI of mice after administration of $Gd@C_{82}(OH)_{22\pm2}$ nanoparticles in doses of 6.5 μmol/kg body weight. (g) MRI of mice after administration of Gd-DTPA at ~130 μmol/kg body weight. In (e), (f), and (g), kidneys images are indicated by arrows. All MR imaging was carried out at 25 °C on a Bruker 4.7 T/30 cm Biospec magnetic resonance imaging scanner.

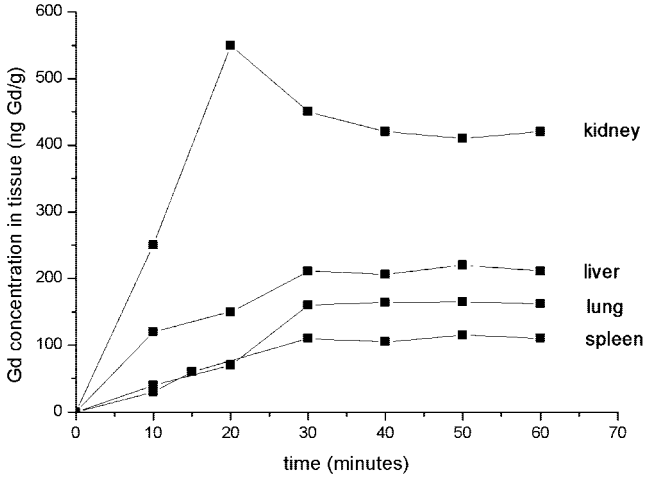

Figure 4. Biodistribution of Gd in the kidney, liver, lung, and spleen in mice at different times after administration of $Gd@C_{82}(OH)_{22\pm2}$ nanoparticles.

2), the negative charges of the $Gd@C_{82}(OH)_{22\pm2}$ particles decrease, and the repulsive electric-static force among particles declines. The strong hydrophobic force and the weaker repulsive electric force work together to push $Gd@C_{82}(OH)_{22\pm2}$ to quickly aggregate together, thus disturbing the self-assembly process and forming large nanoparticles with disordered microstructures (see Figure 1d and e).

In vitro, the proton relaxation of $Gd@C_{82}(OH)_{22\pm2}$ nanoparticles at different pHs (pH 2 and 7) and Gd-DTPA were studied and compared by a T1-weighted spin−echo method under the same conditions (see Supporting Information S9). Note that only the pH 2 and 7 samples of the $Gd@C_{82}(OH)_{22\pm2}$ nanoparticles were selected in the following studies because our attentions are focused on how the microstructure of the nanoparticle affects MRI and because these samples represent the worst (pH 2) and best (pH 7) samples. The longitudinal relaxation rate of $Gd@C_{82}(OH)_{22\pm2}$ at pH 2 and 7 and Gd-DTPA are shown in Figure 2a, b, and c, respectively. Comparing at the same Gd concentration, the r_1 values are 5.2 mM^{-1} s^{-1} for Gd-DTPA, 37.7 mM^{-1} s^{-1} (pH 2), and 61 mM^{-1} s^{-1} (pH 7) for $Gd@C_{82}(OH)_{22\pm2}$ nanoparticles, respectively. The proton relaxivity of $Gd@C_{82}(OH)_{22\pm2}$ particles at pH 7 is about 12× that of Gd-DTPA in vitro.

Interestingly, the $Gd@C_{82}(OH)_{22\pm2}$ nanoparticle (pH 7) with an ordered microstructure has a higher relaxivity of r_1 ~ 61.1 mM^{-1} sec^{-1}, but nanoparticles (pH 2) with disordered structures have lower values of r_1 ~ 37.7 mM^{-1} s^{-1}. This may be attributed to the microstructure difference between $Gd@C_{82}(OH)_{22\pm2}$ nanoparticles. It is reasonable that when the paramagnetic molecules self-organize into an ordered microstructure, it would largely enhance the local magnetic moment of the formed particles when a foreign magnetic field is applied; such nanoparticles will enhance the relaxation for the water proton in MR imaging.[16–19] The saturation magnetic moment of $Gd@C_{82}(OH)_{22\pm2}$ paramagnetic nanoparticles (pH 2 and 7) were studied on a Quantum Design MPMS-XL5 SQUID system at 20 K under −80 000 Oe and 80 000 Oe fields (Supporting Information S9). The curves in the Supporting Information Figure S9 clearly show that the paramagnetic $Gd@C_{82}(OH)_{22\pm2}$ nanoparticles have a saturation magnetic moment of 2.304 emu/g for the pH 7 sample but only of 1.802 emu/g for the pH 2 sample. The magnetic moments are significantly different, indicating that the microstructure has a strong impact on the magnetic properties.

In vitro, the T1-weighted MRI of Gd-DTPA and the $Gd@C_{82}(OH)_{22\pm2}$ nanoparticle phantom were also carried to check their MRI signal directly (S10 in the Supporting Information). Two Gd-DTPA samples were fixed at 0.05 and 1 mM, and the $Gd@C_{82}(OH)_{22\pm2}$ nanoparticle samples (pH 2 and 7) were all 0.05 mM. The nanoparticle at pH 2 showed a weak MRI signal (Figure 3a), but it became much stronger at pH 7 (Figure 3b). Figure 3c reveals that the 0.05 mM Gd-DTPA has the weakest MRI signal when compare with that of the 0.05 mM $Gd@C_{82}(OH)_{22\pm2}$ nanoparticle either at pH 2 or pH 7. The MRI signals of the commercial Gd-DTPA (1 mM) are shown

in Figure 3d. Only when the dose was 20× higher did the Gd-DPTA give similar MR signals to that of $Gd@C_{82}(OH)_{22\pm2}$ at 0.05 mM and pH 7. These studies further confirm that the MRI signals of three samples at the same Gd concentration are in the order $Gd@C_{82}(OH)_{22\pm2}$ nanoparticles (pH 7) > $Gd@C_{82}(OH)_{22\pm2}$ nanoparticles (pH 2) > Gd-DTPA.

For the in vivo MRI studies, a group of mice (ca. 20 g, male, 2 months) were i.v. administrated via the tail vein with $Gd@C_{82}(OH)_{22\pm2}$ (pH 7 particles) in doses of 6.5 μmol/kg body weight. The other two groups were i.v. administrated with Gd-DTPA doses of 6.5 and 130 μmol/kg body weight. Note that the pH 2 sample of $Gd@C_{82}(OH)_{22\pm2}$ is not biocompatible for the in vivo study. Then, the mice were pictured on the MRI scanner (see S11 in the Supporting Information). Figure 3e shows T1-weighted MRI of mice before i.v. administration of the contrast agent; the contrast of the kidney images is very weak. In contrast, in the mice treated with a dose of 6.5 μmol/kg body weight $Gd@C_{82}(OH)_{22\pm2}$ nanoparticle (Figure 3f) and 130 μmol/kg body weight Gd-DTPA (Figure 3g), stronger contrast images of the mice kidney were obtained. Though the dose of Gd-DTPA (130 μmol/kg; Figure 3g) was 20× higher than that of the nanoparticle (6.5 μmol/kg, Figure 3f), the results of MRI imaging showed no significant difference. For the Gd-DTPA at 6.5 μmol/kg body weight, the MRI signal of the kidney was close to that of the control mice without Gd administration; see Figure S11 in the Supporting Information. Compared with traditional Gd-DTPA, these results revealed that $Gd@C_{82}(OH)_{22\pm2}$ nanoparticles (pH 7) have a stronger MR imaging signal in vivo.

To study the biodistribution of $Gd@C_{82}(OH)_{22\pm2}$ nanoparticles in vivo, we used inductively coupled plasma mass spectrometry (ICP-MS) and $Gd@C_{82}(OH)_{22\pm2}$ nanoparticles (pH 7, ~65 nm) in mice. The time-dependent Gd concentration in the liver, spleen, lung, and kidney of the mice were carefully studied (see S12 in the Supporting Information). Note that particles taken up by the RES were mainly located in the liver, lung, and spleen but not in the kidney. Figure 4 shows the time-dependent Gd concentration in the kidney, liver, lung, and spleen in mice. Compared with ~450 ng/g Gd in the kidney, the Gd in liver, lung, and spleen was about ~200, ~170, and ~120 ng/g, respectively. Obviously, the biodistribution of Gd is mainly concentrated in the kidney. It is known that many magnetic nanoparticles have a good MRI signal in vitro, but in vivo, they can be easily recognized by the RES system due to their large size and quickly excrete out the body; thus, it is not applicable in clinical applications.[7–10] At this point, the low uptake by the RES of the $Gd@C_{82}(OH)_{22\pm2}$ nanoparticles is an advantage for in vivo MRI. It is known that small size, normally below 100 nm, and the hydrophilic surface of nanoparticles are key factors for them to escape the RES system.[20,21] Our $Gd@C_{82}(OH)_{22\pm2}$ nanoparticles (pH 7) have a size of ~65 nm, and their hydrophilic hydroxyl groups make them dissolve well in aqueous solution, which may be beneficial for them to escape RES in vivo.

In summary, we developed a method to prepare the $Gd@C_{82}(OH)_{22\pm2}$ paramagnetic nanoparticle. In vitro/vivo MRI studies revealed the same fact; the ordered microstructure of $Gd@C_{82}(OH)_{22\pm2}$ is beneficial for enhancing the proton relaxivity of MRI. In addition, the results suggest that the $Gd@C_{82}(OH)_{22\pm2}$ nanoparticle with a size below 100 nm could successfully escape the RES uptake in vivo, which shows significant advantage for clinical MRI applications.

Acknowledgment. We are thankful for funding support from NSFC (10525524, 10675141, 20571076), the 973 Program (2006CB705601, 2007CB935604), CAS (KJC-NM2007), and CAS Knowledge Innovation Program. The MRI studies were finished with the help of Prof. Hao Lei at the Wuhan Institute of Physics and Mathematics, Chinese Academy of Science.

Supporting Information Available: The methods to synthesize and characterize $Gd@C_{82}(OH)_{22}$ and control the self-assembly of $Gd@C_{82}(OH)_{22\pm2}$ in aqueous solution and AFM, HRTEM, SAXS, MRI, and magnetic studies of samples. This information is available free of charge via the Internet at http://pubs.acs.org

References and Notes

(1) Kato, H.; Kanazawa, Y.; Okumura, M.; Taninaka, A.; Yokawa, T.; Shinohara, H. *J. Am. Chem. Soc.* **2003**, *125*, 4391.
(2) Bolskar, R. D.; Benedetto, A. F.; Husebo, L. O.; Price, R. E.; Jackson, E. F.; Wallace, S.; Wilson, L. J.; Alford, J. M. *J. Am. Chem. Soc.* **2003**, *125*, 5471.
(3) Masahito, M.; Haruhito, K.; Masafumi, O.; Michiko, N.; Yoko, K.; Naoto, M.; Hisanori, S. *Bioconjugate Chem.* **2001**, *12*, 510.
(4) Sitharaman, B.; Bolskar, R. D.; Rusakova, I.; Wilson, L. J. *Nano Lett.* **2004**, *4*, 2373.
(5) Laus, S.; Sitharaman, B.; Toth, E.; Bolskar, R. D.; Helm, L.; Asokan, S.; Wong, M. S.; Wilson, L. J.; Merbach, A. E. *J. Am. Chem. Soc.* **2005**, *127*, 9368.
(6) Okumura, M.; Mikawa, M.; Yokawa, T.; Kanazawa, Y.; Kato, H.; Shinohara, H. *Acad. Radiol.* **2002**, *9*, S495.
(7) Lanza, G. M.; Winter, P. M.; Caruthers, S. D.; Morawsk, A. M.; Schmieder, A. H.; Crowder, K. C.; Wickline, S. A. *J. Nucl. Cardiol.* **2004**, *11*, 733.
(8) Knauth, M.; Egelhof, T.; Roth, S. U.; Wirtz, C. R.; Sartor, K. *Am. J. Neuroradiol.* **2001**, *22*, 99.
(9) Moore, A.; Weissleder, R.; Bogdanov, A., Jr *J. Magn. Reson. Imaging* **1997**, *7*, 1140.
(10) Weissleder, R.; Stark, D. D.; Engelstad, B. L.; Bacon, B. R.; Compton, C. C.; White, D. L.; Jacobs, P.; Lewis, J. *Am. J. Roentgenol.* **1989**, *152*, 167.
(11) Saini, S.; Stark, D. D.; Hahn, P. F.; Wittenberg, J.; Brady, T. J.; Ferrucci, J. T., Jr *Radiology* **1987**, *162*, 211.
(12) Weissleder, R.; Elizondo, G.; Wittenberg, J.; Lee, A. S.; Josephson, L.; and Brady, T. J. *Radiology* **1990**, *175*, 494.
(13) Xing, G. M.; Zhang, J.; Zhao, Y. L.; Tang, J.; Zhang, B.; Gao, X. F.; Yuan, H.; Qu, L.; Cao, W. B.; Chai, Z. F.; Ibrahim, K.; Su, R. *J. Phys. Chem. B* **2004**, *108*, 11473.
(14) Zhang, J.; Liu, K.; Xing, G.; Ren, T.; Wang, S. *J. Radioanal. Nucl. Chem.* **2007**, *272*, 605.
(15) Tagmatarchis, N.; Taninaka, A.; Shinohara, H. *Chem. Phys. Lett.* **2002**, *355*, 226.
(16) Seo, W. S.; Lee, J. H.; Sun, X. M.; Suzuki, Y.; Mann, D.; Liu, Z.; Terashima, M.; Yang, P. C.; Mcconnell, M. V.; Nishimura, D. G.; Dai, H. *Nat. Mater.* **2006**, *5*, 971.
(17) Byrne, S. J.; Corr, S. A.; Gun'ko, Y. K.; Kelly, J. M.; Brougham, D. F.; Ghoshb, S. *Chem. Commun.* **2004**, 2560.
(18) Roch, A.; Muller, R. N.; Gillis, P. *J. Chem. Phys.* **1999**, *110*, 5403.
(19) Sun, S. H.; Fullerton, E. E.; Weller, D.; Murray, C. B. *IEEE. Trans. Magn.* **2001**, *37*, 1239.
(20) Oyewumi, M. O.; Yokel, R. A.; Jay, M.; Coakley, T.; Mumper, R. J. *J. Controlled Release* **2004**, *95*, 613.
(21) Gaur, U.; Sahoo, S. K.; De Tapas, K.; Ghosh, P. C.; Maitra, A.; Ghosh, P. K. *Int. J. Pharm.* **2002**, *202*, 1.

JP8012706